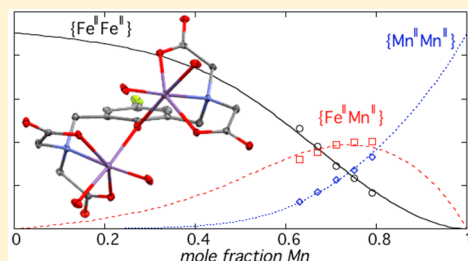


Enhanced Stability of the Fe^{II}/Mn^{II} State in a Synthetic Model of Heterobimetallic Cofactor AssemblyWilliam D. Kerber,^{*,†} Joshua T. Goheen,[†] Kaitlyn A. Perez,[†] and Maxime A. Siegler[‡][†]Department of Chemistry, Bucknell University, Lewisburg, Pennsylvania 17837, United States[‡]Department of Chemistry, Johns Hopkins University, Baltimore, Maryland 21218, United States

Supporting Information

ABSTRACT: Heterobimetallic Mn/Fe cofactors are found in the R2 subunit of class Ic ribonucleotide reductases (R2c) and R2-like ligand binding oxidases (R2lox). Selective cofactor assembly is due at least in part to the thermodynamics of M^{II} binding to the apoprotein. We report here equilibrium studies of Fe^{II}/Mn^{II} discrimination in the biomimetic model system H₅(F-HXTA) (5-fluoro-2-hydroxy-1,3-xylene- α,α' -diamine-*N,N,N',N'*-tetraacetic acid). The homobimetallic F-HXTA complexes [Fe(H₂O)₆][1]₂·14H₂O and [Mn(H₂O)₆][2]₂·14H₂O (**1** = [Fe^{II}₂(F-HXTA)(H₂O)₄]⁻; **2** = [Mn^{II}₂(F-HXTA)(H₂O)₄]⁻) were characterized by single crystal X-ray diffraction. NMR data show that **1** retains its structure in solution (**2** is NMR silent). Metal exchange is facile, and the heterobimetallic complex [Fe^{II}Mn^{II}(F-HXTA)(H₂O)₄]⁻ (**3**) is formed from mixtures of **1** and **2**. ¹⁹F NMR was used to quantify **1** and **3** in the presence of excess M^{II}(aq) at various metal ratios, and equilibrium constants for Fe^{II}/Mn^{II} discrimination were calculated from these data. Fe^{II} is preferred over Mn^{II} with $K_1 = 182 \pm 13$ for complete replacement (**2** \rightleftharpoons **1**). This relatively modest preference is attributed to a hard–soft acid–base mismatch between the divalent cations and the polycarboxylate ligand. The stepwise constants for replacement are $K_2 = 20.1 \pm 1.3$ (**2** \rightleftharpoons **3**) and $K_3 = 9.1 \pm 1.1$ (**3** \rightleftharpoons **1**). $K_2 > K_3$ demonstrates enhanced stability of the heterobimetallic state beyond what is expected for simple Mn^{II} \rightarrow Fe^{II} replacement. The relevance to Fe^{II}/Mn^{II} discrimination in R2c and R2lox proteins is discussed.



INTRODUCTION

Protein metallocofactors play an important and diverse role in nature and range in complexity from single metal ions to large multimetallic clusters.¹ Multinuclear metallocofactors are intriguing because metal ions in close proximity may work cooperatively together to accomplish otherwise difficult chemical transformations.² These cofactors may be assembled from other proteins (metallochaperones)³ or from small-molecule complexes found in labile cellular metal pools.⁴ Frequently the mechanism of metallocofactor assembly is uncertain. Self-assembly of metallocofactors *in vitro* from apoenzymes and solvated metal ions is often possible, although care must be taken to avoid mismetalation.^{2c,5} It is of course still possible for metallochaperones to be involved *in vivo*, but it seems plausible in these cases that the thermodynamics of metal–ligand interactions in the protein active site play an important role in cofactor assembly.

One such example is class I ribonucleotide reductases (RNRs), which catalyze the conversion of RNA to DNA.^{2a} The R2 subunit contains a dinuclear metallocofactor, bound by carboxylate and histidine residues at the center of a four helix bundle, which uses O₂ to generate a radical that is transferred to the active site of the R1 subunit. Class I RNRs are divided into three subclasses based on the identity of the R2 subunit and its bimetallic cofactor:⁵ class Ia utilizes iron, class Ib utilizes manganese, and the more recently discovered class Ic contains a heterobimetallic Fe/Mn cofactor.⁶ Class Ic RNR (R2c) was

originally identified in the pathogen *Chlamydia trachomatis* based on the replacement of a tyrosine residue, normally oxidized to a tyrosyl radical, with a redox inactive phenylalanine.⁷ The Mn/Fe cofactor was eventually identified, and the extra oxidizing equivalent from the missing organic radical was found to be stored on Mn.⁸ A family of ligand-binding oxidases homologous with R2c (R2lox) was subsequently discovered.⁹ R2lox has been structurally characterized in *Mycobacterium tuberculosis* and *Geobacillus kaustophilus* and is thought to be involved in fatty acid biosynthesis. Although the protein structure is modified to create a larger substrate-binding pocket, the heterobimetallic Mn/Fe cofactor in R2lox proteins is conserved.

In vitro metalation of both *Ct* R2c and *Gk* R2lox has been investigated, and the thermodynamics of metal binding play a role in each case.^{9c,10} Both apoenzymes initially load divalent metal ions with at least partial discrimination for the correct {Mn^{II}₍₁₎Fe^{II}_{(2)}} cofactor (Figure 1). A cooperative binding scheme has been proposed for *Gk* R2lox: site 1 is disordered in the apoprotein and is not loaded until Fe^{II} preferentially binds to site 2. In contrast, metal binding in *Ct* R2c does not appear to be cooperative. Both *Ct* R2c sites are ordered in the apoprotein and are sterically isolated by a phenylalanine residue. In the presence of both metals *Ct* R2c selectively

Received: October 7, 2015

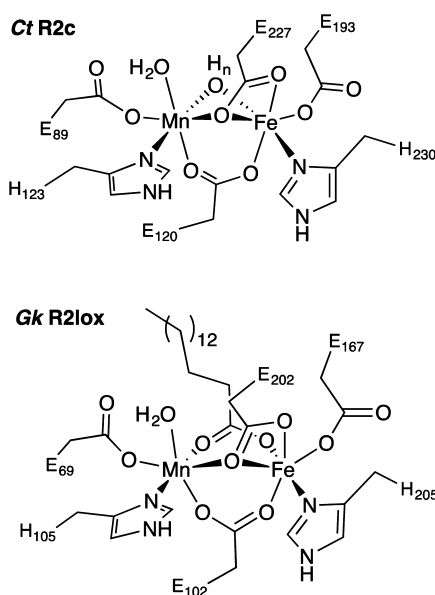
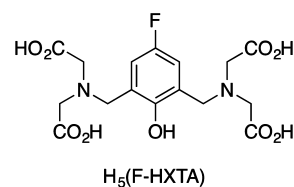


Figure 1. Schematic drawing of the reduced $\{\text{Mn}^{\text{II}}_{(1)}\text{Fe}^{\text{II}}_{(2)}\}$ active sites in *C. trachomatis* R2c protein and *G. kaustophilus* R2lox homologue 1 protein.

assembles $\{\text{Mn}^{\text{II}}_{(1)}\text{Fe}^{\text{II}}_{(2)}\}$ while *Gk* R2lox loads a mixture of $\{\text{Mn}^{\text{II}}_{(1)}\text{Fe}^{\text{II}}_{(2)}\}$ and $\{\text{Fe}^{\text{II}}_{(1)}\text{Fe}^{\text{II}}_{(2)}\}$. The metal ions are substitutionally labile in the reduced state and become fixed in place after O_2 activation.¹¹ Kinetic selectivity plays a role in *Gk* R2lox loading as faster oxidation of $\{\text{Mn}^{\text{II}}_{(1)}\text{Fe}^{\text{II}}_{(2)}\}$ drives the system toward the correct heterobimetallic cofactor.

Although a definitive explanation for $\text{Mn}^{\text{II}}/\text{Fe}^{\text{II}}$ discrimination in *Ct* R2c and *Gk* R2lox remains elusive, it is clear that both proteins are tuned to bias metal binding equilibria toward the correct $\{\text{Mn}^{\text{II}}_{(1)}\text{Fe}^{\text{II}}_{(2)}\}$ cofactor. This is a particularly impressive achievement given the similarity of the residues in the binding sites and the properties of the metal ions.¹² Fe^{II} and Mn^{II} both tend to form high-spin octahedral complexes that are substitutionally labile, but Fe^{II} complexes have greater ligand field stabilization energy (LFSE) because of an additional valence electron (d^6 vs d^5). Fe^{II} also has a slightly smaller ionic radius. The net result is that Fe^{II} usually forms stronger bonds than Mn^{II} , as observed in the classic Irving–Williams series. Both metals are borderline-hard Lewis acids with a preference for Lewis bases such as imidazole and pyridine. In mononuclear complexes, the thermodynamic preference for Fe^{II} over Mn^{II} is well established,¹³ and the same general trend is expected to be true for dinuclear complexes, although fewer examples are known.¹⁴ What is not clear is the stability of the $\text{Fe}^{\text{II}}/\text{Mn}^{\text{II}}$ state relative to the homobimetallic species. The few known examples of synthetic $\text{Fe}^{\text{II}}/\text{Mn}^{\text{II}}$ complexes have been prepared by exploiting nonequilibrium conditions to avoid formation of undesirable homobimetallic species.¹⁵ Given the importance of metal exchange equilibria in R2c and R2lox proteins, we sought to develop a synthetic model system from which $\text{Fe}^{\text{II}}/\text{Mn}^{\text{II}}$ binding could be quantified. The F-HXTA platform (Chart 1) was chosen because, like the binding sites in R2c and R2lox, it is dominated by hard carboxylate donors and because dinuclear HXTA complexes with other M^{II} cations are known.¹⁶ The symmetry of F-HXTA makes the two binding sites identical, which allows the heterobimetallic complex to be investigated without the added complexity of coordination isomers. A method for quantifying paramagnetic F-HXTA complexes by

Chart 1. Dinucleating Ligand Used to Model Metal Binding to R2c/R2lox Proteins



^{19}F NMR was developed to measure equilibrium constants for $\text{Fe}^{\text{II}}/\text{Mn}^{\text{II}}$ discrimination. Our model shows only a modest preference for Fe^{II} , which means Mn^{II} can compete effectively for the ligand binding sites at similar concentrations. We also observed a preference for the heterobimetallic $\text{Fe}^{\text{II}}/\text{Mn}^{\text{II}}$ complex that is greater than predicted by simple $\text{Mn} \rightarrow \text{Fe}$ replacement. Both of these observations support the proposed mechanisms of cofactor assembly in R2c and R2lox proteins. Cytoplasmic concentrations of Fe^{II} and Mn^{II} are similar, and therefore weak discrimination is necessary to load both metals simultaneously.^{4c} An intrinsic preference for the heterobimetallic state is also beneficial because selective loading of Fe^{II} into site 2 will then help direct Mn^{II} to site 1.

RESULTS

The dinucleating ligand 5-fluoro-2-hydroxy-1,3-xylene- α,α' -diamine- N,N,N',N' -tetraacetic acid, $\text{H}_5(\text{F-HXTA})$, was synthesized by Mannich alkylation of 4-fluorophenol with iminodiacetic acid. Homobimetallic F-HXTA complexes were prepared by addition of MCl_2 (3 equiv; $\text{M} = \text{Fe}, \text{Mn}$) and NaOH (5 equiv) to $\text{H}_5(\text{F-HXTA})$. The resultant colorless solutions were slightly basic (pH 7–8) and air sensitive. Exposure of both Fe^{II} and Mn^{II} F-HXTA complexes to O_2 produced darkly colored, uncharacterized products. In the case of iron, the UV–vis spectrum of the oxidized product displayed a strong absorption at 360 nm and a weak shoulder at 500 nm, which is analogous to the spectrum reported for diferric complexes of Me-HXTA.¹⁷ Under anaerobic conditions, the complex anion $[\text{M}^{\text{II}}_2(\text{F-HXTA})(\text{H}_2\text{O})_4]^-$ (**1**, $\text{M} = \text{Fe}$; **2**, $\text{M} = \text{Mn}$) crystallized with $[\text{M}(\text{H}_2\text{O})_6]^{+2}$ to yield colorless single crystals suitable for X-ray structure determination. Displacement ellipsoid plots of **1** and **2** are shown in Figure 2. Crystallographic data are given in Table 1 along with selected bond lengths and angles in Table 2.

Crystals of $[\text{Fe}(\text{H}_2\text{O})_6][\text{1}]_2 \cdot 14\text{H}_2\text{O}$ and $[\text{Mn}(\text{H}_2\text{O})_6][\text{2}]_2 \cdot 14\text{H}_2\text{O}$ were isolated in an anaerobic chamber and dried over P_2O_5 for 1 week. Elemental analyses (C,H,N) on replicate samples were consistent with the loss of 22 water molecules in both cases. The isolated products are therefore formulated as $[\text{M}(\text{H}_2\text{O})_6][\text{M}^{\text{II}}_2(\text{F-HXTA})]_2$ (**1'**, $\text{M} = \text{Fe}$; **2'**, $\text{M} = \text{Mn}$) with the six remaining waters shown in the complex cation, although other coordination isomers are of course possible. Dissolution of **1'** in D_2O gave a colorless solution, and the ^1H NMR spectrum shown in Figure 3a was recorded. Resonances are broad and dispersed over 170 ppm because of the paramagnetic Fe^{II} atoms.¹⁸ Seven peaks of equal area are consistent with the C_2 symmetry of **1** observed in the solid state. Paramagnetic line broadening obscures geminal CH_2 coupling and three-bond H-F coupling. Longitudinal relaxation time constants (T_1) are given in Table 3, along with values calculated from the crystal structure of **1**.¹⁹ The ^{19}F NMR spectrum of **1'** shows a single broad resonance at -74.3 ppm (Figure S4 in the Supporting Information). Identical ^1H and ^{19}F spectra were obtained when **1** was prepared *in situ* from a mixture of $\text{H}_5(\text{F-HXTA})$, FeCl_2 ,

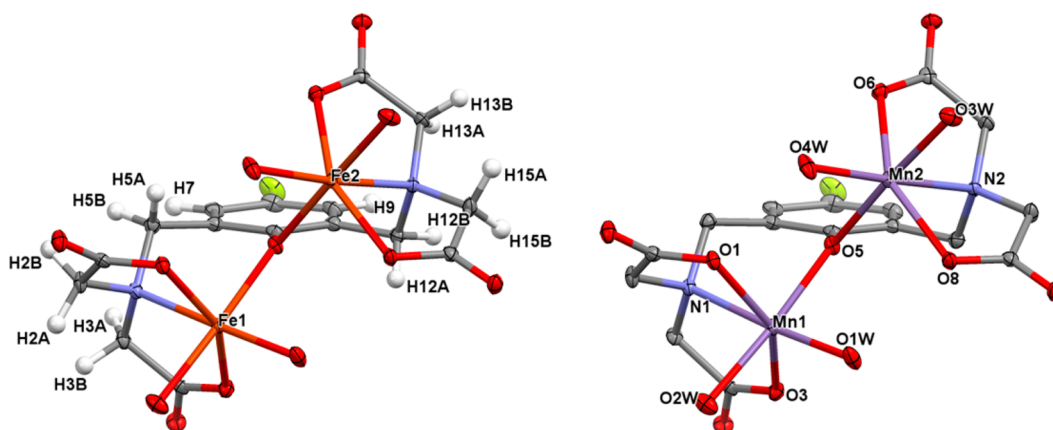


Figure 2. Displacement ellipsoid plots of $[M^{II}_2(F\text{-HXTA})(H_2O)_4]^-$ anions (**1**, $M = \text{Fe}$; **2**, $M = \text{Mn}$). F-HXTA hydrogen atoms are shown to aid assignment of NMR spectra. The same atom-labeling scheme is used consistently for both complexes.

Table 1. Crystallographic Data for $[\text{Fe}(\text{H}_2\text{O})_6][1]_2 \cdot 14\text{H}_2\text{O}$ and $[\text{Mn}(\text{H}_2\text{O})_6][2]_2 \cdot 14\text{H}_2\text{O}$

	$[\text{Fe}(\text{H}_2\text{O})_6][1]_2 \cdot 14\text{H}_2\text{O}$	$[\text{Mn}(\text{H}_2\text{O})_6][2]_2 \cdot 14\text{H}_2\text{O}$
Crystal Data		
empirical formula	$\text{C}_{32}\text{H}_{84}\text{F}_2\text{Fe}_5\text{N}_4\text{O}_{46}$	$\text{C}_{32}\text{H}_{84}\text{F}_2\text{Mn}_5\text{N}_4\text{O}_{46}$
formula wt	1578.28	1573.73
cryst syst	triclinic	triclinic
space group	$P\bar{1}$	$P\bar{1}$
<i>a</i> [Å]	10.8238(3)	10.8657(4)
<i>b</i> [Å]	11.3967(3)	11.4436(4)
<i>c</i> [Å]	13.4092(4)	13.5006(4)
α (deg)	92.709(2)	92.535(3)
β (deg)	113.420(3)	113.243(3)
γ (deg)	90.301(2)	90.364(3)
<i>V</i> (Å ³)	1515.61(8)	1540.43(10)
<i>Z</i>	1	1
<i>T</i> (K)	110(2)	110(2)
cryst size (mm ³)	0.26 × 0.20 × 0.16	0.16 × 0.11 × 0.09
μ (mm ⁻¹)	1.290	1.116
Data Collection		
<i>T</i> _{min} / <i>T</i> _{max}	0.794, 0.860	0.883, 0.927
measd reflns	27964	23903
unique reflns	6967	7077
obsd reflns [<i>I</i> > 2σ(<i>I</i>)]	6627	6433
<i>R</i> _{int}	0.034	0.031
(sin θ/λ) _{max} (Å ⁻¹)	0.650	0.650
Refinement		
<i>R</i> [<i>F</i> ² > 2σ(<i>F</i> ²)]	0.031	0.030
<i>wR</i> (<i>F</i> ²)	0.072	0.069
<i>S</i>	1.05	1.11
params (restraints)	488 (42)	488 (42)
$\Delta\rho_{\text{max}}$ $\Delta\rho_{\text{min}}$ (e Å ⁻³)	0.93, -0.62	0.77, -0.33

and NaOD. A titration of F-HXTA with FeCl_2 monitored by ^{19}F NMR is shown in Figure S5. At substoichiometric Fe^{II} concentrations, a second resonance was observed at -84.7 ppm. This species, which decreased with increasing iron concentration, is attributed to a mononuclear $\text{Fe}^{II}(\text{F-HXTA})$ complex. When 2 equiv of Fe^{II} was added, only the dinuclear complex **1** was observed. In contrast to **1'**, the ^1H spectrum of **2'** dissolved in D_2O showed only a broad solvent resonance, and the ^{19}F spectrum was completely featureless. The slower electronic relaxation rate of Mn^{II} compared with Fe^{II} causes line

Table 2. Selected Bond Lengths and Angles for $[M^{II}_2(\text{F-HXTA})(\text{H}_2\text{O})_4]^-$ (1**, $M = \text{Fe}$; **2**, $M = \text{Mn}$)**

	1	2
Bond Lengths (Å)		
M1–N1	2.2016(19)	2.2783(17)
M2–N2	2.2113(19)	2.2935(17)
M1–O5	2.1025(16)	2.1415(14)
M2–O5	2.0943(16)	2.1332(14)
M1–O3	2.1039(17)	2.1535(14)
M2–O6	2.1127(16)	2.1500(15)
M1–O1	2.1599(16)	2.2414(14)
M2–O8	2.1260(16)	2.1940(14)
M1–O1W	2.0880(17)	2.1345(16)
M2–O4W	2.0742(17)	2.1252(16)
M1–O2W	2.1861(17)	2.2083(16)
M2–O3W	2.1829(17)	2.2111(15)
Bond Angles (deg)		
M1–O5–M2	129.58(7)	127.58(6)
N1–M1–O5	91.04(7)	88.59(6)
N2–M2–O5	91.30(7)	88.93(6)
N1–M1–O2W	90.29(7)	90.97(6)
N2–M2–O3W	89.90(7)	90.14(6)
O5–M1–O1W	87.33(7)	88.34(6)
O5–M2–O4W	89.37(7)	90.95(6)
O1W–M1–O2W	91.37(7)	91.84(6)
O3W–M2–O4W	89.68(7)	90.16(6)
O1–M1–O3	152.63(6)	148.97(5)
O6–M2–O8	153.09(6)	149.39(5)

broadening so extreme that **2** is effectively NMR silent.¹⁸ Solution magnetic susceptibility measurements were made on isolated samples of **1'** and **2'** dissolved in D_2O using the Evans method.²⁰ The effective magnetic moments (μ_{eff}) were found to be $12.4\mu_{\text{B}}$ for **1'** and $13.5\mu_{\text{B}}$ for **2'**. These measurements agree with the theoretical values of μ_{eff} calculated for complexes containing five noninteracting high-spin M^{II} ions ($12.05\mu_{\text{B}}$ for Fe^{II} and $13.23\mu_{\text{B}}$ for Mn^{II}).²¹

A metal ion exchange experiment was performed by dissolving approximately equimolar amounts of **1'** and **2'** in D_2O . The heterobimetallic complex $[\text{FeMn}(\text{F-HXTA})(\text{D}_2\text{O})_4]^-$ (**3**) was expected to form if metal exchange is facile. The ^1H NMR spectrum of this mixture is shown in Figure 3b; **1** is clearly still present, and a new set of resonances has emerged that is consistent with **3**. NMR can usually resolve $\text{Mn}^{II}/\text{Fe}^{II}$

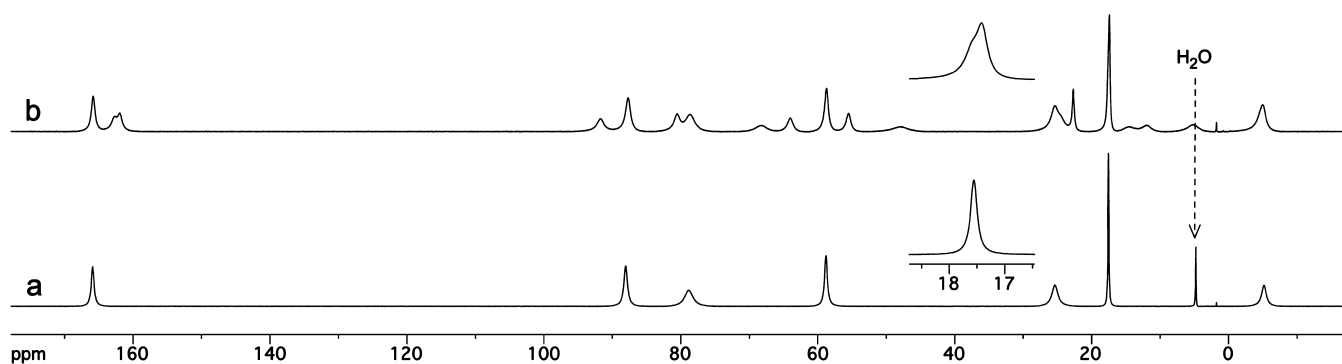


Figure 3. ^1H NMR spectra of isolated $[\text{M}(\text{H}_2\text{O})_6][\text{M}_2(\text{F-HXTA})_2]$ complexes dissolved in D_2O . (a) $[\text{Fe}_2(\text{F-HXTA})(\text{D}_2\text{O})_4]^-$ from **1'**; (b) a mixture of **1'** and **2'** gives $[\text{Fe}_2(\text{F-HXTA})(\text{D}_2\text{O})_4]^-$ and $[\text{FeMn}(\text{F-HXTA})(\text{D}_2\text{O})_4]^-$ after metal ion exchange; $[\text{Mn}_2(\text{F-HXTA})(\text{D}_2\text{O})_4]^-$ is present but not observed. Presaturation was used to suppress residual H_2O in both spectra. Inset: one of the aryl protons of **3** overlaps with **1**.

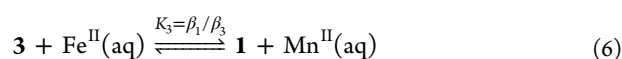
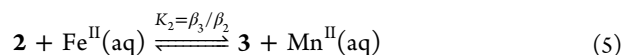
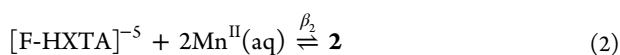
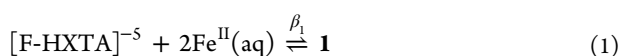
Table 3. ^1H -NMR Data for Isolated $[\text{Fe}(\text{H}_2\text{O})_6][\text{Fe}_2(\text{F-HXTA})_2]$ (**1'**) Dissolved in D_2O

protons ^a	position ^b	δ (ppm)	$\nu_{1/2}$ ^c (Hz)	T_1 , obsd ^d (ms)	T_1 , calcd ^e (ms)
H5B, H12B	eq	165.9	187	2.1	2.4
H2B, H15B	eq	88.0	244	2.3	2.2
H5A, H12A	ax	78.9	443	0.63	0.59
H3A, H13A	eq	58.8	197	2.4	2.1
H3B, H13B	ax	25.4	294	1.0	1.3
H7, H9		17.6	64	9.4	
H2A, H15A	ax	-5.2	336	1.1	0.95

^aAtom labeling scheme from Figure 2. ^bAxial-like or equatorial-like disposition in the chelate ring. ^cLine width at half height. ^dMeasured by inversion–recovery. ^eCalculated relative to $T_1(\text{H}_7/\text{H}_9)$ using H/Fe distances from the crystal structure of **1**; see ref 19 and Supporting Information for a discussion.

complexes because magnetic coupling to Fe^{II} increases the electronic relaxation rate of Mn^{II} .^{15c,18} Complex **3** has C_1 symmetry and therefore twice as many ^1H resonances as **1**. A ^{19}F NMR spectrum of the **1'**/**2'** mixture was recorded, and a new resonance attributed to **3** is seen at -65.5 ppm. (Figure S6 in the Supporting Information). ^{19}F NMR was also used to investigate the kinetics of metal ion exchange: The amount of **3** increased for about 2 h after mixing, and then the peak area ratios remained constant. Identical equilibrium mixtures could be prepared *in situ* from $\text{H}_3(\text{F-HXTA})$, FeCl_2 , MnCl_2 , and NaOD .

The speciation of F-HXTA in the presence of both Fe^{II} and Mn^{II} is governed by the equilibria shown in eqs 1–3. Although we have not measured the individual stability constants β_{1-3} , they must be relatively large because there is no evidence for free ligand or mononuclear $\text{M}^{\text{II}}(\text{F-HXTA})$ complexes at stoichiometric metal loadings. Equations 4–6 describe F-HXTA speciation in the presence of excess M^{II} , with K_{1-3} defining the relative stabilities of the three bimetallic complexes.



We have evaluated K_{1-3} in a series of metal competition experiments by preparing equilibrium mixtures of F-HXTA with excess $\text{FeCl}_2/\text{MnCl}_2$ at pH 7.29(3). The concentrations of **1** and **3** were measured directly by ^{19}F NMR and the concentrations of **2**, $\text{Fe}^{\text{II}}(\text{aq})$, and $\text{Mn}^{\text{II}}(\text{aq})$ were calculated from mass balance equations. Although K_{1-3} may be determined at a single Fe/Mn ratio, we repeated the experiment at multiple ratios to test our proposed speciation model. The results were averaged to give $K_1 = 182 \pm 13$, $K_2 = 20.1 \pm 1.3$, and $K_3 = 9.1 \pm 1.1$. Data are shown in Figure 4; the

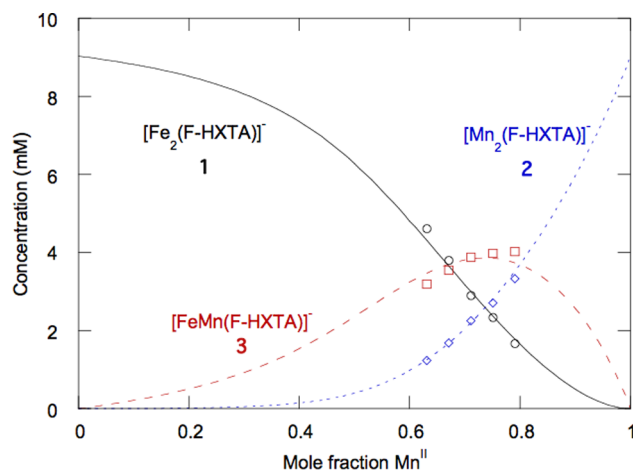


Figure 4. Concentrations of **1** (O), **2** (□), and **3** (□) as a function of $\text{Fe}^{\text{II}}/\text{Mn}^{\text{II}}$ ratio. $[\text{F-HXTA}] = 9.03(5)$ mM; $[\text{MCl}_2]_{\text{total}} = 40.16(9)$ mM; pH = 7.29(3). Curves are calculated from K_{1-3} (this work) and β_{MCl^+} (ref 22).

open symbols are concentrations measured by experiment, and the curves are concentrations calculated from K_{1-3} and the formation constants for $[\text{FeCl}]^+(\text{aq})$ and $[\text{MnCl}]^+(\text{aq})$.²² The complete data set, including individual NMR spectra, is given in the Supporting Information.

Conditions for metal competition experiments were chosen such that all species were present above 1 mM. All samples were equilibrated at 25 °C for 24 h prior to analysis, and pH was maintained at 7.29(3) with buffered *N*-methylmorpholine (NMM). NMM was chosen because its steric bulk inhibits

metal ion coordination, which was confirmed when identical NMR spectra were obtained from unbuffered solutions manually adjusted to pH 7.3 with NaOH. Identical spectra were also obtained when FeCl_2 was replaced with $\text{Fe}(\text{NH}_4)_2(\text{SO}_4)_2$. Because pH and MCl_2 concentration were held constant, all measurements were made at the same ionic strength ($I = 0.111 \text{ M}$) and activity coefficients were neglected. 4-Fluorophenol (4-FP) was used as an internal standard for ^{19}F NMR and its presence did not affect the peak area ratio of 1/3. Although 4-FP did exhibit paramagnetic line broadening and faster relaxation ($T_1 = 60\text{--}80 \text{ ms}$ depending on Mn/Fe ratio), its chemical shift was unaffected. These data indicate the 4-FP does not form metal complexes to a significant degree at the low concentrations employed in this work.

DISCUSSION

F-HXTA Complexes in the Solid State. Single crystals of $[\text{Fe}(\text{H}_2\text{O})_6][\text{I}]_2 \cdot 14\text{H}_2\text{O}$ and $[\text{Mn}(\text{H}_2\text{O})_6][\text{2}]_2 \cdot 14\text{H}_2\text{O}$ suitable for X-ray structure determination were isolated, and the two complexes share nearly identical crystal lattices. The small differences observed are attributable to slightly but statistically longer metal–ligand bonds in **2** versus **1** ($\Delta_{\text{M-L}} = 0.022\text{--}0.082 \text{ \AA}$). The largest difference in bond lengths is observed with the amine ($\Delta_{\text{M1-N1}} = 0.079 \text{ \AA}$; $\Delta_{\text{M2-N2}} = 0.082 \text{ \AA}$) and the carboxylates lying in the plane of the phenolate ($\Delta_{\text{M1-O1}} = 0.082 \text{ \AA}$; $\Delta_{\text{M2-O8}} = 0.068 \text{ \AA}$). Complexes **1** and **2** have approximate C_2 symmetry, with the aromatic ring canted from the M1–O5–M2 plane by 52.2° in **1** and 53.6° in **2**. Each metal atom is found in a distorted octahedral geometry. The angles in those octahedra range from 76.5° to 108.1° for **1** and from 74.6° to 105.4° for **2**. The metal atoms are displaced from mean square planes (defined by N1, O1W, O2W, and O5 and N2, O3W, O4W, and O5) by ca. 0.05 and 0.03 \AA in **1** and ca. 0.08 and 0.01 \AA in **2**. The carboxylate ligands are *trans* across the square planes, with substantial deviations from linearity observed in the O1–M1–O3 and O6–M2–O8 angles; $152.63(6)^\circ$ and $153.09(6)^\circ$ for **1** and $148.97(5)^\circ$ and $149.39(5)^\circ$ for **2**.

Drying the isolated crystals caused loss of 22 of 28 water molecules in both cases. The formulation of these products as $[\text{M}(\text{H}_2\text{O})_6][\text{M}_2(\text{F-HXTA})]_2$ (**1'**, $\text{M} = \text{Fe}$; **2'**, $\text{M} = \text{Mn}$) is convenient but probably not entirely accurate. Other coordination isomers are possible, and it also seems likely in the solid state that at least some of the sites vacated by water are reoccupied by bridging interactions with ligands from adjacent complex ions. Regardless, the observation that NMR spectra of **1'** are identical to samples prepared *in situ* indicates that hydration of the isolated material regenerates $[\text{Fe}^{II}_2(\text{F-HXTA})(\text{H}_2\text{O})_4]^-$ in solution. This is presumably true of **2'** as well, although the Mn^{II} complex is NMR silent.

F-HXTA Complexes in Solution. The ^1H NMR spectrum of isolated **1'** exhibits seven resonances of equal intensity, consistent with a C_2 symmetric F-HXTA ligand as observed in the solid state. Although Fe^{II} is substitutionally labile, chelation slows ligand exchange sufficiently that fluxional behavior on the NMR time scale is not observed. Our data is consistent with the structurally similar diiron(II) complex, $[\text{Fe}_2(\text{BPMP})(\mu\text{-O}_2\text{P}(\text{O}(\text{Ph})_2)_2)_2]^+$ (BPMP = 2,6-bis[(bis(2-pyridylmethyl)amino)-methyl]-4-methylphenol), which has been thoroughly characterized by 1-D and 2-D ^1H NMR.¹⁹ Coupling of electron and nuclear magnetic moments disperses the proton resonances for **1** over 170 ppm and produces substantial line broadening by providing an efficient mechanism for nuclear relaxation.¹⁸ The

hyperfine shift (the paramagnetic contribution to the chemical shift) and nuclear relaxation time constants (T_1 and T_2) are affected by dipolar contributions from unpaired metal electrons, and by contact contributions from spin density delocalized onto the resonating nuclei. Dipolar coupling of protons to a magnetically anisotropic metal like high-spin Fe^{II} is orientation dependent, but the interaction is averaged by molecular motion. The averaged dipolar shift is therefore isotropic and is more properly called a pseudocontact shift. Because dipolar coupling is distance dependent, hyperfine shifts, line widths, and relaxation times are all a rough measure of proton–metal distance. The aromatic protons in **1** (H7/9) are the furthest from Fe^{II} and are easily assigned to the resonance at 17.6 ppm by their narrower line width, longer T_1 , and smaller hyperfine shift. The CH_2 groups in **1** are found in chelate rings with protons in equatorial-like and axial-like positions. The equatorial protons are further from the metal and therefore have narrower line widths and longer T_1 times than the axial protons.¹⁹ This is evidenced by the three sharp and three broad CH_2 resonances in Figure 3a and three long ($\geq 2.1 \text{ ms}$) and three short ($\leq 1.1 \text{ ms}$) T_1 times in Table 3. Proton–metal distances from the crystal structure of **1** were also used to calculate T_1 times, and these values are in good agreement with the experimentally determined time constants (see Supporting Information for a discussion of this procedure). The CH_2 hyperfine shifts are more difficult to interpret because of the dependence of the contact contribution on the Fe–N–C–H dihedral angle, but a given equatorial proton is generally shifted further downfield than its axial partner.¹⁸ Taken together the chemical shifts, line widths, and T_1 times allow the tentative assignments of CH_2 protons shown in Table 3.

Dinuclear Fe^{II}_2 and Mn^{II}_2 complexes in hard ligand fields are generally high-spin and exhibit weak magnetic coupling.^{9c,23} Magnetic susceptibility measurements on solutions of **1'** and **2'** are consistent with this trend, and the complexes are described as ensembles of noninteracting high-spin M^{II} ions. The formation of **3** from a mixture **1'** and **2'** demonstrates that $\text{M}^{II}(\text{aq})$ exchange with $[\text{M}_2(\text{F-HXTA})(\text{H}_2\text{O})_4]^-$ is facile. The ^{19}F NMR spectrum of the mixture shows a single resonance each for **1** and **3** (Figure S6). The ^1H spectrum is more difficult to interpret because **3** has 14 unique F-HXTA protons (Figure 3b). The aryl protons in **3** are relatively sharp and easy to identify, but unlike **1**, separate resonances are expected for H7 and H9. One of these protons is clearly seen at 22.4 ppm, and examination of the inset in Figure 3b shows that the other overlaps with the H7/9 signal from **1**. The 12 broad CH_2 resonances are present but not readily assigned. Similar spectra have been reported for $\text{Mn}^{II}(\mu\text{-OAr})\text{Fe}^{II}$ clusters supported by other dinucleating ligands,¹⁵ and the isolectronic $\text{Fe}^{II}/\text{Fe}^{III}$ complex $[\text{Fe}_2(\text{Me-HXTA})(\mu\text{-OAc})_2]^{-2,24}$.

$\text{Fe}^{II}/\text{Mn}^{II}$ Exchange Equilibria. Paramagnetic ^{19}F NMR has increasingly been used to investigate both metalloproteins and synthetic model systems.²⁵ We employed ^{19}F NMR to measure equilibrium concentrations of paramagnetic F-HXTA complexes because of the better resolution and fewer lines compared with ^1H spectra. Equilibrium constants for $\text{Fe}^{II}/\text{Mn}^{II}$ exchange show that Fe^{II} binds more strongly than Mn^{II} (K_{1-3}). Although this trend is typical, the magnitude of the preference is relatively small. Complete metal ion replacement for a bimetallic complex (eq 4) is equal to the sum of the stepwise reactions (eqs 5 and 6) and $K_1 = K_2K_3$. For comparison to mononuclear complexes, we will define the $\text{Fe}^{II}/\text{Mn}^{II}$ discrimination constant ($\beta_{\text{Fe}}/\beta_{\text{Mn}}$) as $\sqrt{K_1} = 13$, or

the average equilibrium constant for a single $\text{Mn}^{\text{II}} \rightarrow \text{Fe}^{\text{II}}$ substitution. EDTA (ethylenediamine tetraacetate) is structurally similar to F-HXTA, and $[\text{M}^{\text{II}}(\text{EDTA})]^{-2}$ also shows a modest preference for Fe^{II} ($\beta_{\text{Fe}}/\beta_{\text{Mn}} = 1.4$).²⁶ Fe^{II} affinity increases dramatically with pyridine ligands, for example, $\beta_{\text{Fe}}/\beta_{\text{Mn}} = 1.5 \times 10^4$ for $[\text{M}^{\text{II}}(\text{pic})_3]^{-}$ (pic = pyridine-2-carboxylate).²⁷ The trend continues for complexes with only pyridyl donors: $[\text{M}^{\text{II}}(\text{bpy})_3]^{+2}$ (bpy = 2,2'-bipyridine) has a $\text{Fe}^{\text{II}}/\text{Mn}^{\text{II}}$ discrimination constant 10 orders of magnitude greater than F-HXTA ($\beta_{\text{Fe}}/\beta_{\text{Mn}} = 5.4 \times 10^{11}$).²⁸ Hard–soft acid–base theory (HSAB) provides an explanation for these data. Both Fe^{II} and Mn^{II} are moderately hard Lewis acids that form strong bonds with similar Lewis bases, such as pyridine and imidazole. Maximizing metal–ligand orbital overlap with a good HSAB match increases $\beta_{\text{Fe}}/\beta_{\text{Mn}}$ by magnifying the effect of the differences between the two metals (LFSE, ionic radii, d^6 vs d^5 geometric preferences). Conversely, a HSAB mismatch with very hard carboxylate ligands minimizes these differences and produces a small $\text{Fe}^{\text{II}}/\text{Mn}^{\text{II}}$ discrimination factor because the slightly harder Mn^{II} ion competes more effectively with Fe^{II} for available metal binding sites.

The relationship between K_2 and K_3 determines the relative stability of the heterobimetallic complex **3**. If the two metal binding sites in F-HXTA were completely independent from one another, each $\text{Mn}^{\text{II}} \rightarrow \text{Fe}^{\text{II}}$ substitution would be isoenergetic and the stepwise replacement constants would be equal ($K_3 = K_2 = \sqrt{K_1}$). If this were true, the preference for Fe^{II} could be explained by the same arguments used for mononuclear complexes. Although these factors are certainly still important, the observation that $K_2 > K_3$ (20.1 ± 1.3 vs 9.1 ± 1.1) indicates an additional favorable interaction in **3** specific to the heterobimetallic state. Since the crystal structures of **1** and **2** are nearly identical, it is reasonable to assume that **3** would be similar as well, which means there is not a substantial change in ligand geometry that can be used to explain the observed stability enhancement. $\text{M}^{\text{II}}(\mu\text{-OR})\text{M}^{\text{II}}$ clusters of Fe^{II} and Mn^{II} ions generally experience weak antiferromagnetic coupling for both homo- and heteronuclear combinations,^{9c,23} so differences in magnetic coupling do not provide an obvious explanation for the stability of **3**. Because K_2 is only slightly larger than K_3 , only a relatively small steric or electronic effect is necessary to create the observed bias toward **3**, but as discussed below for *Ct* R2c and *Gk* R2lox, even a small effect may be important for heterobimetallic cofactor assembly.

Speciation Model Selection. Equations 4–6 outline a relatively simple speciation model that assumes complete formation of anionic $[\text{M}^{\text{II}}_2(\text{F-HXTA})]^{-}$ complexes in the presence of excess $\text{M}^{\text{II}}(\text{aq})$. Each species is an aggregate of multiple states (protonation, chloride complexation), and in order to calculate K_{1-3} it must be assumed that the composition of these states is invariant across all Fe/Mn ratios. Calculating the expected concentrations of **1–3** from K_{1-3} (the curves in Figure 4) is a way to test this assumption. A slight systematic error between the measured and calculated concentrations is apparent in Figure 4, and although the discrepancy is small enough to not affect the conclusion that $K_2 > K_3$,²⁹ further discussion of the speciation model is warranted.

All samples were buffered at pH 7.29, and protonation equilibria were neglected. This is reasonable for $[\text{M}(\text{H}_2\text{O})_6]^{+2}$ because the vanishingly small hydrolysis constants ($\log \beta_{\text{FeOH}^+} = -9.88$; $\log \beta_{\text{MnOH}^+} = -10.59$)³⁰ cause an insignificant change when included in the speciation model. If the aquo ligands in **1–3** have comparable acidities, their hydrolysis is also safely

neglected. On the other hand, protonation of carboxylate residues in **1–3** should be considered because this has been observed in the solid state for other $\text{M}^{\text{II}}_2(\text{HXTA})$ complexes.^{16a} Unbuffered solutions prepared from $\text{H}_5(\text{F-HXTA})$, MCl_2 , and stoichiometric NaOH (5 equiv) generally had a pH of 7–8 suggesting the metal complexes are very weakly basic. Nevertheless, if the $\text{p}K_a$ of $\text{H}[\text{M}(\text{F-HXTA})(\text{H}_2\text{O})_4]$ varies slightly with metal identity, a small systematic error in the calculated concentrations of **1–3** will be introduced.

The effect of chloride in the reaction medium is more significant. MCl_2 salts were utilized because they are available in high purity for both metals and it was desirable to keep the counterion identity constant. Chloride is a coordinating anion, and the concentration of $[\text{M}(\text{H}_2\text{O})_5\text{Cl}]^+$ is not negligible, but fortunately it does not vary much with the $\text{Fe}^{\text{II}}/\text{Mn}^{\text{II}}$ ratio because the formation constants for the two metals are similar ($\log \beta_{\text{FeCl}^+} = -0.16$; $\log \beta_{\text{MnCl}^+} = -0.61$).²² When β_{FeCl^+} and β_{MnCl^+} were included in the speciation model, the calculated fraction of the total metal pool found as $[\text{M}(\text{H}_2\text{O})_5\text{Cl}]^+$ varied from 2.9% to 1.1% as the mole fraction of Mn^{II} varied from 0 to 1. This change makes a small difference in the calculated concentrations of **1–3** and is at least partially responsible for the systematic error seen in Figure 4. Chloride may also coordinate directly to F-HXTA complexes, but the importance of species like $[\text{M}^{\text{II}}_2(\text{F-HXTA})(\text{H}_2\text{O})_3\text{Cl}]^{-2}$ cannot be determined from our data. The magnitude of the effect is probably smaller than for $\text{M}^{\text{II}}(\text{aq})$ because addition of Cl^- to anionic $[\text{M}^{\text{II}}_2(\text{F-HXTA})]^{-}$ complexes is presumably less favorable than addition to dicationic hexaquo ions.

Relevance to Protein Cofactor Assembly. Comparison of the active sites of *Ct* R2c and *Gk* R2lox with the crystal structures of **1** and **2** shows that F-HXTA is a reasonable small-molecule analog of the natural systems. The metal ions in **1** and **2** are found in distorted octahedrons with a single neutral nitrogen donor and five anionic oxygen donors, creating a hard ligand field that exhibits a relatively modest ability to discriminate between Fe^{II} and Mn^{II} . This HSAB mismatch also causes Fe^{II} and Mn^{II} F-HXTA complexes to oxidize very rapidly in air. *Ct* R2c and *Gk* R2lox contain six-coordinate metal ions as well, each with one neutral nitrogen donor (histidine) and a collection of anionic oxygen donors (carboxylates and possibly hydroxide in the case of *Ct* R2c). This abundance of hard Lewis bases has interesting consequences for the assembly of bimetallic cofactors in *Ct* R2c and *Gk* R2lox proteins. The catalytically active forms of both enzymes contain high-valent metals that are stabilized by a hard ligand field,¹¹ but the metals are loaded in the divalent state. This creates a HSAB mismatch between the metal ions and the binding site during cofactor assembly, which in the case of simple coordination compounds reduces the $\text{Fe}^{\text{II}}/\text{Mn}^{\text{II}}$ discrimination factor ($\beta_{\text{Fe}}/\beta_{\text{Mn}}$). Because cytoplasmic concentrations of Fe^{II} and Mn^{II} are similar,^{4c} carboxylate-rich binding sites should enhance competitive formation of $\{\text{Mn}^{\text{II}}\text{Fe}^{\text{II}}\}$ cofactors.

Equilibrium binding of $\text{Mn}^{\text{II}}/\text{Fe}^{\text{II}}$ mixtures to apoenzymes has been investigated for both *Ct* R2c and *Gk* R2lox. Griese et al.^{9c} reported crystal-soaking experiments of metal-free *Gk* R2lox in excess M^{II} at a 1:1 Fe/Mn ratio. Analysis of the metal content by X-ray anomalous dispersion revealed that site 1 contained approximately equimolar amounts of each metal while site 2 contained excess Fe^{II} in about a 4:1 ratio. In terms of macroscopic selectivity, *Gk* R2lox preferentially binds Fe^{II} in a 65:35 ratio from a 1:1 mixture of aqueous metal salts. This level of M^{II} discrimination is comparable to our model system:

Under similar conditions,³¹ F-HXTA preferentially binds Fe^{II} in an 83:17 ratio. Equilibrium binding to Ct R2c has been reported by Dassama et al.¹⁰ at stoichiometric M^{II} loadings (2 equiv per polypeptide; 1:1 Fe/Mn ratio). Macroscopic discrimination cannot be determined at these conditions (the bound Fe/Mn ratio is necessarily 1:1 if all sites are occupied), but a very strong microscopic preference for the {Mn^{II}₍₁₎Fe^{II}₍₂₎} cofactor was observed. In fact, within the limits of detection by X-ray anomalous dispersion, Mn^{II} was found exclusively in site 1 and Fe^{II} exclusively in site 2. Although stoichiometric M^{II} also maximizes the concentration of 3 in our model,³² the impressive thermodynamic preference for the heterobimetallic cofactor in Ct R2c is clearly greater than that in F-HXTA.

The explanation for selective formation of a {Mn^{II}₍₁₎Fe^{II}₍₂₎} cofactor in R2c and R2lox proteins has been discussed extensively. What is particularly intriguing is the mechanism by which site 1 subverts the usual preference for Fe^{II} over Mn^{II}. A comparison of binding sites in a series of RNR R2 class Ia, b, and c proteins by Dassama et al.¹⁰ suggests that Mn^{II} selectivity may result from the presence of exogenous water ligands that allow a more flexible coordination geometry. Similar arguments have been made for small-molecule coordination complexes that prefer Mn^{II} to Fe^{II}.¹³ Chelating ligands that enforce a subtle distortion or a reduction in coordination number may alter metal binding preference.³³ A rigid binding pocket can select the slightly larger Mn^{II} cation in favor of the smaller Fe^{II} cation.³⁴ Although there are probably many contributing factors to selective cofactor assembly in R2c and R2lox proteins, our results suggest a new possibility should be investigated: Binding of Mn^{II} in site 1 may be affected by the presence of Fe^{II} in site 2, not just through the rearrangement of residues in the adjacent site^{9c} but also through an intrinsic favorable interaction between the metal ions in a {Mn^{II}Fe^{II}} cluster.

CONCLUSIONS

Equilibrium binding of Fe^{II}/Mn^{II} mixtures to the dinucleating ligand F-HXTA was used as a chemical model of heterobimetallic cofactor loading in R2c and R2lox proteins. Homobimetallic species containing the complex anion [M^{II}₂(F-HXTA)(H₂O)₄]⁻ (1, M = Fe; 2, M = Mn) were characterized by single crystal X-ray diffraction. The two structures are nearly identical except for small differences attributed to slightly longer bonds for Mn^{II}. The complexes are small-molecule analogs of R2c and R2lox proteins with each metal in a distorted octahedral ligand field dominated by hard carboxylate residues. NMR data shows that 1 retains its structure in solution, and the same is presumed for 2 although the Mn^{II} complex is NMR silent. The heterobimetallic variant 3 is formed from mixtures of 1 and 2, demonstrating that M^{II} exchange in F-HXTA complexes is facile. Metal competition experiments were performed using ¹⁹F NMR to measure the concentrations of 1 and 3 at various Fe^{II}/Mn^{II} ratios and equilibrium constants for Fe^{II}/Mn^{II} exchange were determined. Complete replacement of Mn^{II} with Fe^{II} is favorable ($K_1 = 182 \pm 13$ for $2 \rightleftharpoons 1$), but the magnitude of the preference is relatively small. This is attributed to a HSAB mismatch between the carboxylate ligands in F-HXTA and divalent transition metal ions. This demonstrates how a binding site dominated by carboxylate residues may be advantageous for heterobimetallic proteins like R2c and R2lox by allowing the usually less favorable {Mn^{II}Fe^{II}} cofactor to compete with {Fe^{II}Fe^{II}}. The relative stability of the heterobimetallic complex 3 was assessed by comparison of stepwise Mn^{II} → Fe^{II} equilibrium constants

($K_2 = 20.1 \pm 1.3$ for $2 \rightleftharpoons 3$; $K_3 = 9.1 \pm 1.1$ for $3 \rightleftharpoons 1$). The fact that K_2 is greater than K_3 indicates that there is an additional favorable interaction in 3 specific to the heterobimetallic state. Although there are not any obvious steric or electronic explanations for this effect in the F-HXTA model, if found to be generally true for Mn^{II}/Fe^{II} complexes, this effect provides another explanation for how proteins like R2c and R2lox can selectively assemble heterobimetallic cofactors. We are currently investigating the stability of Fe^{II}/Mn^{II} complexes in other ligand fields, including a nonsymmetric F-HXTA derivative that will mimic the high and low affinity sites in R2c and R2lox proteins.

EXPERIMENTAL PROCEDURES

General. Aqueous solutions were prepared from Type 1 ultrapure water with a resistivity of at least 18 MΩ·cm⁻¹. FeCl₂·4H₂O from Strem was stored under N₂(g), and anhydrous MnCl₂ from Alfa Aesar was stored in a desiccator. N-Methylmorpholine from Aldrich was distilled from sodium metal under N₂(g). 4-Fluorophenol from Aldrich was sublimed under vacuum when used as an internal standard. All other reagents were obtained from Aldrich or Acros and used as received.

Fe^{II} and Mn^{II} complexes of F-HXTA are air sensitive and were prepared and handled in a COY Laboratories anaerobic chamber containing <1 ppm of O₂. All solvents and liquid reagents were freeze–pump–thaw degassed prior to use. NMR samples in D₂O were sealed in J-Young-style NMR tubes. NMR samples in mixed H₂O/D₂O media were frozen in liquid nitrogen and flame-sealed under vacuum in medium wall NMR tubes. Crystallization samples were frozen in liquid nitrogen and flame-sealed under vacuum in glass storage ampules. **Caution!** While no problems were encountered in this work, flame-sealing vessels in liquid nitrogen may create an explosion hazard. Always confirm that no gases have condensed in the vessel prior to sealing and allow the samples to thaw completely behind a blast shield.

5-Fluoro-2-hydroxy-1,3-xylene- α,α' -diamine-N,N,N',N'-tetraacetic acid, H₅(F-HXTA). A solution of 0.616 g of NaOH (15.4 mmol) in 2.63 mL of H₂O was cooled in an ice bath, and 1.051 g of iminodiacetic acid (7.90 mmol) was added. After complete dissolution, 0.444 g of 4-fluorophenol (3.96 mmol) was added followed by 0.369 g of paraformaldehyde (12.3 mmol). The cloudy yellow solution was warmed to room temperature and then heated to 50 °C. After heating for 48 h, the homogeneous orange solution was diluted with 23 mL of methanol and cooled in an ice bath. The crude product was precipitated with 0.320 mL of 12.1 M HCl (3.87 mmol). The solid was isolated by filtration and dried under vacuum to yield 1.189 g (ca. 2.54 mmol) of Na₃H₂(F-HXTA). The crude product was dissolved in 12.7 mL of H₂O and addition of 3.13 mL of 2.42 M HCl (7.57 mmol) caused H₅(F-HXTA) to crystallize slowly at room temperature. The solid was isolated by filtration and dried under vacuum to yield 0.914 g (2.27 mmol, 57%) of pale yellow crystals. ¹H NMR (DMSO, 400 MHz): δ 6.96 (d, 2H, ³J_{HF} = 9.2 Hz), 3.83 (s, 4H), 3.43 (s, 8H). ¹⁹F NMR (DMSO, 376 MHz): δ -128.5 (t, ³J_{FH} = 9.2 Hz, ¹J_{FC} = 234 Hz). ¹³C{¹H} NMR (DMSO, 100 MHz) δ 172.5, 155.0 (d, ¹J_{CF} = 233 Hz), 151.1, 125.0, 114.6 (d, ³J_{CF} = 22 Hz), 54.0, 53.0. Anal. Calcd for C₁₆H₁₉FN₂O₉: C, 47.77; H, 4.76; N, 6.96. Found: C, 47.48; H, 4.69; N, 6.88.

[Fe(H₂O)₆][Fe₂(F-HXTA)(H₂O)₄]₂·14H₂O. In an anaerobic chamber, 67 mg of H₅(F-HXTA) (0.17 mmol) was dissolved in 1.49 mL of H₂O with 0.670 mL of NaOH (0.995 M, 0.666 mmol), and to this solution was added 0.960 mL of FeCl₂ (0.5221 M, 0.501 mmol). The solution was titrated to pH 7.13 with 0.975 mL of NaOH (0.166 M, 0.162 mmol). A fine blue precipitate formed immediately and was removed with a 0.45 μm nylon syringe filter. The supernatant was frozen in liquid nitrogen and sealed in a glass ampule. The product precipitated after thawing, but heating to 50 °C caused it to redissolve. The homogeneous solution was stored at 5 °C, and colorless crystals suitable for X-ray structure determination grew in 1 week. The product was isolated by filtration in an anaerobic chamber and dried over P₂O₅.

for 1 week. ^1H NMR (D_2O , 400 MHz): δ 165.9 (br, 2H), 88.0 (br, 2H), 78.9 (br, 2H), 58.8 (br, 2H), 25.4 (br, 2H), 17.6 (br, 2H), -5.2 (br, 2H). ^{19}F NMR (D_2O , 376 MHz): δ -74.3. Anal. Calcd for $\text{C}_{32}\text{H}_{40}\text{F}_2\text{Fe}_3\text{N}_4\text{O}_{24}$ (loss of 22 H_2O): C, 32.52; H, 3.41; N, 4.74. Found: C, 32.28; H, 3.48; N, 4.60.

[Mn(H₂O)₆][Mn₂(F-HXTA)(H₂O)₄]₂·14H₂O. In an anaerobic chamber, 97 mg of $\text{H}_5(\text{F-HXTA})$ (0.24 mmol) was dissolved in 0.970 mL of NaOH (0.995 M, 0.965 mmol), and to this solution was added 1.19 mL of MnCl_2 (0.6086 M, 0.7248 mmol). The solution was titrated to pH 8.42 with 0.780 mL of NaOH (0.291 M, 0.227 mmol). After 2 h, a fine white precipitate had formed, which was removed with a 0.45 μm nylon syringe filter. The supernatant was frozen in liquid nitrogen and sealed in a glass ampule. Colorless crystals suitable for X-ray structure determination grew in 1 week at 5 °C. The product was isolated by filtration in an anaerobic chamber and dried over P_2O_5 for 1 week. Anal. Calcd for $\text{C}_{32}\text{H}_{40}\text{F}_2\text{Mn}_3\text{N}_4\text{O}_{24}$ (loss of 22 H_2O): C, 32.64; H, 3.42; N, 4.76. Found: C, 32.44; H, 3.46; N, 4.46.

Single Crystal X-ray Crystallography. All reflection intensities were measured at 110(2) K using a SuperNova diffractometer (equipped with Atlas detector) with Mo $K\alpha$ radiation ($\lambda = 0.71073$ Å) under the program CrysAlisPro (version 1.171.36.32, Agilent Technologies, 2013). The same program was used to refine the cell dimensions and for data reduction. Structures were solved with the program SHELXS-2013 (Sheldrick, 2008) and refined on F^2 with SHELXL-2013 (Sheldrick, 2008). Analytical numeric absorption correction based on a multifaceted crystal model was applied using CrysAlisPro. The temperature of the data collection was controlled using the system Cryojet (manufactured by Oxford Instruments). The H atoms were placed at calculated positions (unless otherwise specified) using the instructions AFIX 23 or AFIX 43 with isotropic displacement parameters having values $1.2U_{\text{eq}}$ of the attached C atoms. The H atoms of the coordinated (OnW , $n = 1-7$) and lattice (OnW , $n = 8-14$) water molecules were found from difference Fourier maps, and their coordinates were refined freely. Both structures are ordered with the $[\text{M}(\text{H}_2\text{O})_6]^{+2}$ cations found at sites of inversion symmetry, thus only one-half of the cation is crystallographically independent. The crystals of **1** and **2** were pseudomerohedrally twinned. Twinning was checked with the TwinRotMat algorithm from Platon.³⁵ The twin relationship corresponds to a 2-fold axis along the a direction with the matrix M : 1 0 0/0 $\bar{1}$ 0/ $\bar{1}$ 0 $\bar{1}$. The BASF scale factors refine to 0.1331(7) for **1** and 0.0416(5) for **2**.

Metal Exchange Experiments. Solutions were prepared by diluting aliquots of aqueous stock solutions to the final target concentrations. Calibrated automatic pipettes and volumetric flasks were used throughout. Because $\text{H}_5(\text{F-HXTA})$ is insoluble in water, stock solutions were prepared as $\text{Na}_3\text{H}_2(\text{F-HXTA})$ by adding 3 equiv of NaOH.

Representative Procedure. To a 5 mL volumetric flask containing 1.000 mL of D_2O was added 1.494 mL of $\text{Na}_3\text{H}_2(\text{F-HXTA})$ (0.03055 M, 0.0456 mmol), 0.400 mL of FeCl_2 (0.2010 M, 0.0804 mmol), 0.598 mL of MnCl_2 (0.2012 M, 0.120 mmol), 0.120 mL of 4-fluorophenol (0.2070 M, 0.0248 mmol), and 0.494 mL of N -methylmorpholine (0.302 M, 0.149 mmol). The flask was diluted to the mark with H_2O . An aliquot of this solution was sealed in an NMR tube and equilibrated at 25.0 °C for 24 h prior to analysis. The pH of the remaining solution was measured after 24 h, and the raw meter reading was adjusted for isotopic composition using the formula $\text{pH}_{\text{actual}} = \text{pH}_{\text{meter}} - n(0.073 \times \text{pH}_{\text{meter}} - 0.42)$ where n is the deuterium mole fraction of the sample.³⁶

NMR Spectroscopy. Spectra were acquired on a Varian 400 MHz DirectDrive spectrometer equipped with a 5 mm ASW PFG probe. Data were processed in iNMR or MNova. Chemical shifts are reported relative to residual solvent resonances for ^1H and ^{13}C and relative to NaPF_6 for ^{19}F . T_1 measurements were made with a calibrated 90° pulse using a standard inversion–recovery pulse sequence. Several changes to standard Varian pulse sequences were necessary for paramagnetic samples: The automatic gradient shimming routine was modified by increasing the number of transients acquired (nt) to 64, decreasing the relaxation delay (d1) to 0.1 s, and decreasing the incremental delay array (d3) to [0, 0.01] s. Acoustic ringing during ^{19}F

acquisition was mitigated by increasing the amplifier blanking delay (rof2) to 40 ms.

Procedure for Equilibrium Measurements. The wide sweep width used in ^{19}F experiments (33.8 kHz) made it impossible to produce a uniform 90° pulse for all three resonances of interest (**1**, **3**, and the internal standard 4-FP). Two acquisitions were performed per sample, varying the transmitter offset frequency to be equidistant from 4-FP and either **1** or **3**. A 90° pulse was calibrated separately for each experiment. A total of 51 200 transients were collected with a total recycle time of 0.48 s (0.08 s acquisition; 0.4 s delay), which was at least 6 \times greater than the longest T_1 (dependent on $\text{Fe}^{\text{II}}/\text{Mn}^{\text{II}}$ ratio). Probe temperature was maintained at 25.0 °C. The FID was zero-filled to 32 000 points, and acoustic ringing was removed in the first four points using backward-linear prediction. Twenty hertz of exponential line broadening was applied, and resonances were integrated over ± 18 times the peak-width at half-height to cover 99% of the area of a Lorentzian distribution.

Speciation Modeling. Concentration curves for **1–3** in Figure 4 were calculated in Hyss2009³⁷ at the following initial conditions: $[\text{Fe}^{\text{II}}] = 40.18-0$ mM; $[\text{Mn}^{\text{II}}] = 0-40.24$ mM; $[\text{F-HXTA}] = 9.03$ mM; $[\text{Cl}^-] = 80.4$ mM. The model used for this calculation consisted of formation constants (β) for **1**, **2**, **3**, $[\text{FeCl}]^+(\text{aq})$, and $[\text{MnCl}]^+(\text{aq})$. β_{1-3} were calculated from K_{1-3} by choosing an arbitrarily large value of β_1 (10^{20}) such that essentially no F-HXTA was present and then calculating relative values of β_2 and β_3 from eqs 4–6. β_{FeCl^+} and β_{MnCl^+} were taken from the literature.²²

Magnetic Susceptibility. Measurements were made at 25 °C using the Evans method adapted to the geometry of superconducting magnets.²⁰ Accurately weighed samples of **1'** and **2'** were dissolved in D_2O in volumetric flasks to a target concentration of ca. 10 mg/mL. The solutions were prepared to contain 1.0 mM *tert*-butanol and were loaded into the outer chambers of coaxial NMR tubes. The inner chamber contained a reference solution of 1.0 mM *tert*-butanol in D_2O . The molar susceptibilities of the dissolved complexes (χ_{M}) were calculated from the equation

$$\chi_{\text{M}} = \text{MW}_{\text{solute}} \left(\chi_0 + \frac{3\Delta\nu}{4\pi\nu_0 c} \right) \quad (7)$$

where $\text{MW}_{\text{solute}}$ is the molecular weight of the metal complex, χ_0 is the mass susceptibility of the solvent D_2O ($-0.65 \times 10^{-6} \text{ cm}^3/\text{g}$), $\Delta\nu$ is the difference in hertz between the *tert*-butanol resonances in the inner and outer chambers, ν_0 is the operating frequency of the spectrometer in hertz, and c is the concentration of the metal complex in grams per milliliter. The paramagnetic contribution to the observed molar susceptibility (χ_{P}) was calculated by subtracting the diamagnetic contribution (χ_{D}) from χ_{M} . Pascal constants were used to estimate χ_{D} for **1'** ($-508 \times 10^{-6} \text{ cm}^3/\text{mol}$) and **2'** ($-513 \times 10^{-6} \text{ cm}^3/\text{mol}$).³⁸ The paramagnetic susceptibilities were used to determine effective magnetic moments (μ_{eff}) expressed in units of the Bohr magneton (μ_{B})

$$\mu_{\text{eff}} = 2.84 \sqrt{\chi_{\text{P}} T} \quad (8)$$

where T is the temperature in Kelvin. These values were compared with the predicted magnetic moments for complexes containing n noninteracting metal ions

$$\mu^2 = g^2 \left(\sum_{i=1}^n S_i(S_i + 1) \right) \quad (9)$$

where g is the Landé factor (2.2 for high-spin Fe^{II} and 2.0 for high-spin Mn^{II}) and S_i is the total electron spin quantum number for each individual metal ion.²¹

■ ASSOCIATED CONTENT

📄 Supporting Information

The Supporting Information is available free of charge on the ACS Publications website at DOI: 10.1021/acs.inorg-

chem.5b02322. CIFs have been deposited in the Cambridge Structural Database.

NMR spectra of $H_5(F\text{-HXTA})$, **1'**, a titration of F-HXTA with $FeCl_2$, and of a **1'**/**2'** mixture. Discussion of the method used to calculate T_1 time constants for **1**, and complete data set and results of F-HXTA metal competition experiments (PDF)

Crystallographic information file (CIF) for **1** (CIF)

Crystallographic information file (CIF) for **2** (CIF)

AUTHOR INFORMATION

Corresponding Author

*E-mail: will.kerber@bucknell.edu.

Notes

The authors declare no competing financial interest.

ACKNOWLEDGMENTS

We are grateful for financial support provided by Bucknell University and the donors of the American Chemical Society Petroleum Research Fund (Grant 50877-UNI3). W.D.K. thanks Dr. David Rovnyak for helpful discussion of quantitative paramagnetic NMR.

REFERENCES

- (1) Crichton, R. R. *Biological Inorganic Chemistry*; Elsevier: Amsterdam, 2012.
- (2) (a) Stubbe, J.; Nocera, D. G.; Yee, C. S.; Chang, M. C. Y. *Chem. Rev.* **2003**, *103*, 2167–2201. (b) Sazinsky, M. H.; Lippard, S. J. *Acc. Chem. Res.* **2006**, *39*, 558–566. (c) Schenk, G.; Mitić, N.; Gahan, L. R.; Ollis, D. L.; McGeary, R. P.; Guddat, L. W. *Acc. Chem. Res.* **2012**, *45*, 1593–1603. (d) Peterson, R. L.; Kim, S.; Karlin, K. D. In *Comprehensive Inorganic Chemistry II*; Reedijk, J. K. P., Ed.; Elsevier: Oxford, 2013; Vol. 3, pp 149–177. (e) Grazina, R.; Pauleta, S. R.; Moura, J. J. G.; Moura, I. In *Comprehensive Inorganic Chemistry II*; Reedijk, J. K. P., Ed.; Elsevier: Oxford, 2013; Vol. 3, pp 103–148.
- (3) (a) Rae, T. D.; Schmidt, P. J.; Pufahl, R. A.; Culotta, V. C.; O'Halloran, T. V. *Science* **1999**, *284*, 805–808. (b) Rosenzweig, A. C. *Chem. Biol.* **2002**, *9*, 673–677. (c) Philpott, C. C. *J. Biol. Chem.* **2012**, *287*, 13518–13523.
- (4) (a) Kakhlon, O.; Cabantchik, Z. I. *Free Radical Biol. Med.* **2002**, *33*, 1037–1046. (b) Tottey, S.; Waldron, K. J.; Firbank, S. J.; Reale, B.; Bessant, C.; Sato, K.; Cheek, T. R.; Gray, J.; Banfield, M. J.; Dennison, C.; Robinson, N. J. *Nature* **2008**, *455*, 1138–1142. (c) Hider, R. C.; Kong, X. L. *BioMetals* **2011**, *24*, 1179–1187.
- (5) (a) Cotruvo, J. A., Jr.; Stubbe, J. *Annu. Rev. Biochem.* **2011**, *80*, 733–767. (b) Stubbe, J.; Cotruvo, J. A., Jr. *Curr. Opin. Chem. Biol.* **2011**, *15*, 284–290. (c) Cotruvo, J. A., Jr.; Stubbe, J. *Metallomics* **2012**, *4*, 1020–1036.
- (6) (a) Griese, J. J.; Srinivas, V.; Högbom, M. *JBIC, J. Biol. Inorg. Chem.* **2014**, *19*, 759–774. (b) Bollinger, J. M., Jr.; Jiang, W.; Green, M. T.; Krebs, C. *Curr. Opin. Struct. Biol.* **2008**, *18*, 650–657. (c) Carboni, M. L.; Latour, J.-M. *Coord. Chem. Rev.* **2011**, *255*, 186–202.
- (7) Högbom, M.; Stenmark, P.; Voevodskaya, N.; McClarty, G. *Science* **2004**, *305*, 245–248.
- (8) (a) Jiang, W.; Yun, D.; Saleh, L.; Barr, E. W.; Xing, G.; Hoffart, L. M.; Maslak, M. A.; Krebs, C.; Bollinger, J. M. *Science* **2007**, *316*, 1188–1191. (b) Voevodskaya, N.; Lenzian, F.; Ehrenberg, A.; Gräslund, A. *FEBS Lett.* **2007**, *581*, 3351–3355. (c) Andersson, C. S.; Öhrström, M.; Popović-Bijelić, A.; Gräslund, A.; Stenmark, P.; Högbom, M. *J. Am. Chem. Soc.* **2012**, *134*, 123–125. (d) Dassama, L. M. K.; Boal, A. K.; Krebs, C.; Rosenzweig, A. C.; Bollinger, J. M., Jr. *J. Am. Chem. Soc.* **2012**, *134*, 2520–2523.
- (9) (a) Andersson, C. S.; Högbom, M. *Proc. Natl. Acad. Sci. U. S. A.* **2009**, *106*, 5633–5638. (b) Högbom, M. *JBIC, J. Biol. Inorg. Chem.* **2010**, *15*, 339–349. (c) Griese, J. J.; Roos, K.; Cox, N.; Shafaat, H. S.; Branca, R. M. M.; Lehtio, J.; Gräslund, A.; Lubitz, W.; Siegbahn, P. E.; Högbom, M. *Proc. Natl. Acad. Sci. U. S. A.* **2013**, *110*, 17189–17194.
- (10) Dassama, L. M. K.; Krebs, C.; Bollinger, J. M., Jr.; Rosenzweig, A. C.; Boal, A. K. *Biochemistry* **2013**, *52*, 6424–6436.
- (11) The oxidized states are believed to be $\{Mn^{IV}_{(1)}Fe^{III}_{(2)}\}$ for Ct R2c and $\{Mn^{IV}_{(1)}Fe^{IV}_{(2)}\}$ for Gk R2lox, see ref 6.
- (12) Cotton, F. A.; Wilkinson, G. *Advanced Inorganic Chemistry*; Wiley: New York, 1988; pp 697–724.
- (13) A search of the IUPAC stability constant database yields 347 entries for ligands with known stability constants for both Fe^{II} and Mn^{II} . In only 20 cases is the corresponding Mn^{II} complex more stable. See <http://www.iupac.org/index.php?id=410> (accessed September 24, 2015).
- (14) Wang, J.; Martell, A. E.; Motikatis, R. J. *Inorg. Chim. Acta* **2001**, *322*, 47–55.
- (15) (a) Tereniak, S. J.; Carlson, R. K.; Clouston, L. J.; Young, V. G., Jr.; Bill, E.; Maurice, R.; Chen, Y.-S.; Kim, H. J.; Gagliardi, L.; Lu, C. C. *J. Am. Chem. Soc.* **2014**, *136*, 1842–1855. (b) Carboni, M.; Clémancey, M.; Molton, F.; Pécaut, J.; Lebrun, C.; Dubois, L.; Blondin, G.; Latour, J. M. *Inorg. Chem.* **2012**, *51*, 10447–10460. (c) Wang, Z.; Holman, T. R.; Que, L., Jr. *Magn. Reson. Chem.* **1993**, *31*, S78–S84. (d) Holman, T. R.; Wang, Z.; Hendrich, M. P.; Que, L., Jr. *Inorg. Chem.* **1995**, *34*, 134–139.
- (16) (a) Laborda, S.; Clérac, R.; Anson, C. E.; Powell, A. K. *Inorg. Chem.* **2004**, *43*, 5931–5943. (b) Meng, B.-H.; Gao, F.; Zhu, M.-L. *Acta Crystallogr., Sect. C: Cryst. Struct. Commun.* **2004**, *60*, m308–m310. (c) Gao, F.; Meng, B.-H.; Wei, Y.-B. *Acta Crystallogr., Sect. C: Cryst. Struct. Commun.* **2004**, *60*, m360–m362. (d) Ma, L.; Lu, L.; Zhu, M.; Wang, Q.; Gao, F.; Yuan, C.; Wu, Y.; Xing, S.; Fu, X.; Mei, Y.; Gao, X. *J. Inorg. Biochem.* **2011**, *105*, 1138–1147.
- (17) Murch, B. P.; Bradley, F. C.; Boyle, P. D.; Papaefthymiou, V.; Que, L., Jr. *J. Am. Chem. Soc.* **1987**, *109*, 7993–8003.
- (18) (a) Bertini, I.; Luchinat, C. *NMR of Paramagnetic Molecules in Biological Systems*; Benjamin/Cummings: Menlo Park CA, 1986. (b) Bertini, I.; Turano, P.; Vila, A. J. *Chem. Rev.* **1993**, *93*, 2833–2932.
- (19) Ming, L. J.; Jang, H. G.; Que, L., Jr. *Inorg. Chem.* **1992**, *31*, 359–364.
- (20) (a) Evans, D. F. *J. Chem. Soc.* **1959**, 2003–2005. (b) Sur, S. K. *J. Magn. Reson.* **1989**, *82*, 169–173.
- (21) Girerd, J.-J.; Journaux, Y. In *Physical Methods in Bioinorganic Chemistry: Spectroscopy and Magnetism*; Que, L., Jr., Ed.; University Science Books: Sausalito, CA, 2000; pp 321–374.
- (22) (a) Heinrich, C. A.; Seward, T. M. *Geochim. Cosmochim. Acta* **1990**, *54*, 2207–2221. (b) Gammons, C. H.; Seward, T. M. *Geochim. Cosmochim. Acta* **1996**, *60*, 4295–4311.
- (23) Que, L., Jr.; True, A. E. *Prog. Inorg. Chem.* **1990**, *38*, 97–200.
- (24) Borovik, A. S.; Murch, B. P.; Que, L., Jr.; et al. *J. Am. Chem. Soc.* **1987**, *109*, 7190–7191.
- (25) Belle, C.; Béguin, C.; Hamman, S.; Pierre, J.-L. *Coord. Chem. Rev.* **2009**, *253*, 963–976.
- (26) Brunetti, A. P.; Nancollas, G. H.; Smith, P. N. *J. Am. Chem. Soc.* **1969**, *91*, 4680–4683.
- (27) Anderegg, G. *Helv. Chim. Acta* **1960**, *43*, 414–424.
- (28) Irving, H.; Mellor, D. H. *J. Chem. Soc.* **1962**, 5222–5237.
- (29) If $K_2 = K_3$, there would necessarily be a Fe^{II}/Mn^{II} ratio that produces equimolar amounts of **1**, **2**, and **3**. Inspection of Figure 4 shows that this is clearly not the case.
- (30) (a) Millero, F. J.; Yao, W.; Aicher, J. *Mar. Chem.* **1995**, *50*, 21–39. (b) Perrin, D. D. *J. Chem. Soc.* **1962**, 2197–2200.
- (31) Initial conditions: 9 mM F-HXTA; 18 mM $FeCl_2$; 18 mM $MnCl_2$. Calculated speciation: 2.62 mM **3**, 5.86 mM **1**, and 0.525 mM **2**.
- (32) Initial conditions: 9 mM F-HXTA; 9 mM $FeCl_2$; 9 mM $MnCl_2$. Calculated speciation: 3.85 mM **3**, 2.58 mM **1**, and 2.58 mM **2**.
- (33) (a) Delgado, R.; Fraústo da Silva, J. J. R.; Vaz, M. C.; Paoletti, P.; Micheloni, M. *J. Chem. Soc., Dalton Trans.* **1989**, 133–137. (b) Paoletti, P.; Ciampolini, M. *Inorg. Chem.* **1967**, *6*, 64–68.
- (34) Miyake, H.; Kato, N.; Kojima, Y.; Sugihara, A. *Inorg. Chim. Acta* **1994**, *223*, 121–124.

- (35) Spek, A. L. *Acta Crystallogr., Sect. D: Biol. Crystallogr.* **2009**, *D65*, 148–155.
- (36) Krężel, A.; Bal, W. *J. Inorg. Biochem.* **2004**, *98*, 161–166.
- (37) (a) Alderighi, L.; Gans, P.; Ienco, A.; Peters, D.; Sabatini, A.; Vacca, A. *Coord. Chem. Rev.* **1999**, *184*, 311–318. (b) Hyperquad Simulation and Speciation (HySS2009), Protonic Software, 2009; <http://www.hyperquad.co.uk/hyss.htm> (accessed September 24, 2015).
- (38) Bain, G. A.; Berry, J. F. *J. Chem. Educ.* **2008**, *85*, 532–536.